Pergamon

Pattern Recognition, Vol. 29, No. 9, pp. 1531–1542, 1996

Printed in Great Britain
0031-3203/96 $15.00 + .00

PII: S0031-3203(96)00006-4

MODELS AND ALGORITHMS FOR A REAL-TIME HYBRID IMAGE ENHANCEMENT METHODOLOGY

CHANCHAL CHATTERJEE* and VWANI P. ROYCHOWDHURY
School of Electrical and Computer Engineering, Purdue University, West Lafayette, IN 47907-1285, U.S.A.

(*Received* 1 *March* 1995; *in revised form* 19 *December* 1995; *received for publication* 11 *January* 1996)

Abstract—The paper presents models and algorithms for a hybrid method of image enhancement. The proposed framework involves processing of the digitized image to transform the input signal from image sensors such that the digitization of the transformed analog signal yields the enhanced image. First, an analytical framework which yields robust algorithms for image enhancement (following our approach) is established. Unlike many conventional methods, the approach allows the user to specify certain statistical measures for desired gray values in the enhanced image. An appealing feature of the proposed method is its ease of implementation using off-the-shelf hardware such as Analog-to-Digital Converters. To support our models and analyses, we perform character recognition on a set of industrial parts. Copyright © 1996 Pattern Recognition Society. Published by Elsevier Science Ltd.

Contrast enhancement Analog-to-Digital Converter Hybrid enhancement

1. INTRODUCTION

In this paper we propose a hybrid method of image enhancement. The method involves processing of the digitized image to obtain a set of enhancing parameters. These parameters are used to transform the input analog signal from image sensors, such that the digitization of the transformed signal is the enhanced image. In particular, our approach allows the user to first select certain statistical measures (such as mean and variance) of desired gray values in the enhanced image. The algorithms process the digitized image to generate parameters to transform the input analog signal by affine functions. The transformed analog signal is digitized to generate the desired enhanced image (Fig. 1).

One of the novelties of the proposed method lies in its analytical models that relate the digitized image to the analog input signal. While most methods enhance the digitized image pixel by pixel, the proposed method uses parameters from the digitized image to reacquire a new enhanced image. Since image acquisition is usually concurrent and faster than image computation, the enhancement process can be realized at near acquisition speeds. Moreover, the models are directly implementable using off-the-shelf hardware such as Analog-to-Digital Converters (ADCs).[1–3] Contributions in this study are:

(1) Given certain statistical measures (mean and variance) of desired gray values, we describe models and algorithms to generate an enhanced image.

(2) Theoretical studies considered in this paper for computational efficiency are implemented to reach real-time speeds without custom hardware.

(3) We provide analytical expressions for upper and lower bounds of the desired gray-value measures that can be obtained without scaling of the image (see Section 3.4).

(4) If the gray-value measure selections exceed these limits, we offer efficient methods of image scaling and also offer parameter feedbacks to the optical system to achieve the desired enhancement (see Section 3.4).

(5) We consider the effects of constant and Gaussian quantization and measurement errors on the estimates of model parameters and on the enhanced image (see Section 4).

(6) The models and analyses are applied to a character recognition application involving a set of industrial parts (see Section 3.5).

1.1. *Description of Fig.* 1

1.1.1. *Input V and Image S.* Let $V \in \mathscr{R}^n$ be an input analog image signal and $S \in \mathscr{R}^n$ be the corresponding gray-scale image, where n is the number of digitized pixels. Note that input V can originate from many sources, such as sensors (cameras, lasers) or stored analog image signals. Let $[v_{\min}, v_{\max}]$ be the full dynamic range of input V and let $[s_{\min}, s_{\max}]$ be the dynamic range of the intensity in S. Define $\Theta = \{v \in \mathscr{R}: v_{\min} \le v \le v_{\max}\}$ and $\Phi = \{s \in \mathscr{R}: s_{\min} \le s \le s_{\max}\}$.

1.1.2. *Regions* $\{R_1, \ldots, R_m\}$. Within S, we identify $m (1 \le m \le n)$ disjoint nonempty regions $\{R_1, \ldots, R_m\}$ to be enhanced. The number of sizes of regions are determined by the application (see Appendix). Each region R_i of S consists of a subset $S_i \subset S$ of contiguous pixels. The analog input corresponding to S_i is denoted by V_i.

*Author for correspondence.

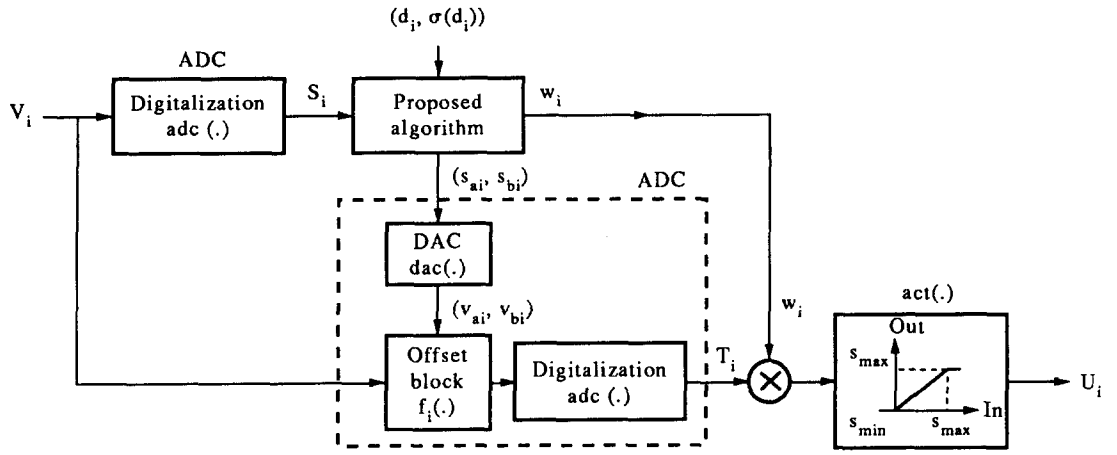

Fig. 1. Interaction of the proposed algorithm to generate enhanced image U_i from analog signal V_i.

1.1.3. *First and second order measures of S_i.* Each S_i consists of gray values $s_{ij}, j = 1, \ldots, n_i$, where n_i is the number of pixels within S_i. We define s_i as a first-order measure of S_i, such as the average, weighted average or random sample. Similarly, we define $\sigma(s_i)$ is a second-order measure of S_i, such as the sample standard deviation or range of intensities about the mean s_i.

1.1.4. *Analog to digital and digital to analog converters.*[1-3] The digitization process in the ADC is a *surjective* map $\Theta \to \Phi$. We consider an ideal ADC as a function $\text{adc}(\cdot): s = cv + e$, where $v \in \Theta$ is an analog signal value that is digitized to a gray value $s \in \Phi$. Here, c is a scalar constant and e is a *nonlinear* quantization error. We shall discuss the effects of e on our algorithm by considering e as a constant value and also as a Gaussian i.i.d. random variable. In analysing our models we have considered many nonidealities in common ADCs. The DAC, defined as a function $\text{dac}(\cdot): \Phi \to \Theta$, is similarly modeled by the above function in the ideal and nonideal cases. Note that the DAC is included in almost all ADC hardware.

1.1.5. *Desired mean gray value d_i and desired standard deviation $\sigma(d_i)$.* For every region R_i, the *user selects a desired mean gray value $d_i \in \Phi$.* Our algorithm automatically generates an enhanced image U, such that the mean u_i of region R_i within U equals d_i for $i = 1, \ldots, m$. Similarly, for every R_i the *user selects a desired standard deviation $\sigma(d_i)$*, such that the standard deviation $\sigma(u_i)$ of the enhanced image U_i equals $\sigma(d_i)$.

1.1.6. *Enhancement parameters and offset block $f_i(\cdot)$.* For each S_i, the algorithm automatically computes a set of digital offsets (s_{ai}, s_{bi}) and weight w_i. The offsets include a low offset s_{ai} and a high offset s_{bi}, which are transformed by the DAC to analog offsets (v_{ai}, v_{bi}). The analog offsets are used to modify the input signal V_i by an affine functions $f_i(\cdot): \Theta \to \Theta$ in the Offset Block of the ADC. The modified input $f_i(V_i)$ is digitized by the ADC to obtain the enhanced image T_i.

1.1.7. *Final enhanced image U.* Enhanced image T_i is multiplied by weight w_i to yield the final image U_i. Since most ADCs do not have a method of multiplying the analog signal, weights w_i are applied to the digital image T_i instead of analog input $f_i(V_i)$. Considering a linear ADC, we have $\text{adc}(w_i f_i(V_i)) = w_i \text{adc}(f_i V_i)) = w_i T_i$. Thus, multiplying the analog signal $f_i(V_i)$ by w_i is the same as multiplying the image T_i. Finally, $w_i T_i$ is clipped to lie within $[s_{\min}, s_{\max}]$ to produce the enhanced image U_i. The union of images $\{U_1, \ldots, U_m\}$ for disjoint regions $\{R_1, \ldots, R_m\}$, respectively, gives us the final enhanced image U.

Note that although the analysis is carried out for the ADC, the general method described above can be applied to any hardware which conforms to functions $f_i(\cdot)$ and $\text{adc}(\cdot)$ defined in our models.

1.2. *Comparison with state of the art*

The many image enhancement methods[4-10] for gray-scale images commonly belong to: (a) spatial domain and (b) frequency domain methods. In both methods enhancement parameters are extracted from the digital image, which are used to modify the original image pixel by pixel to generate an enhanced image. The proposed method, on the other hand, reacquires a new enhanced image with parameters obtained from the digital image.

We have identified the histogram modification[11-21] techniques as the methods closest to ours. Methods in this category belong to (a) global methods, (b) adaptive methods and (c) methods using structure. The global or stationary enhancement techniques involve gray-level transformations based slolely on the intensity of each pixel. Methods include contrast stretching,[4] histogram equalization,[5,9,20,21,22] histogram hyperbolization[15] and histogram specification.[16] Adaptive enhancement methods calculate the

new intensity value for a pixel from its original value and some local image properties. Methods include unsharp masking,[7] statistical difference filter,[18] local histogram modification,[20] pixel contrast measure,[17] adaptive histogram equalization (AHE)[23] and contrast-limited AHE.[24] The final category includes methods that use local image structures to change the enhancement calculation itself or change the contextual region over which the calculations are carried out. For other methods see references (25, 26) and for detailed analyses of all the above methods see references (13, 14, 27).

The results of the region-based global histogram specification methods are similar to the proposed model. However, these methods modify the image pixels by pixel. The adaptive and structure dependent methods are local operations that are suitable for enhancing subtle details at the expense of principal features which may be lost in the process.[16,28,29] For data-intensive applications such as online character recognition,[30,31] the speed and economy of implementation are very important. For example, in order to identify the quality and content of material in blocks of steel, a set of characters are laser etched on them during the manufacturing process. These characters are machine-read online for proper routing and archival. A major drawback of adaptive methods such as local histogram modification "is that it carries a heavy computational burden" and "practically prohibits the use of these techniques on general purpose computers in online or real-time applications".[27]

The advantages of the proposed method are:

(1) Computational efficiency: A significant property of the proposed approach is its execution in near *acquisition speeds*. While speeds of most methods depend on the number of pixels in the image, the speed of this method depends on the acquisition rate, which is usually faster than image computation.

(2) Generation of desired gray-value measures: The proposed method allows the user to *select the desired gray-value measures (mean and variance)* of the enhanced image. In applications where surface qualities of parts change from sample to sample, this algorithm can be used to generate images of the same gray-value distribution for all parts, which can then be processed by a *single image processing algorithm*. Note that local histogram modification methods[20] do allow for desired gray-value generation over regions.

(3) Economy of implementation: A key advantage of this method is that no custom hardware is needed for efficient computation. It can be implemented in any processor that has an ADC.

In Section 2 we shall present ideal and nonideal analytical models for signal transformation with an ADC. In Section 3 we shall discuss the enhancement method with experimental results and also study the extent of enhancement that is possible with weights $w_i = 1$. Error analysis with constant and Gaussian quantization errors is given in Section 4. Section 5 has the concluding remarks.

2. MODELING APPLICATION: A CASE STUDY

In this section we shall consider an implementation of the enhancement model with an ADC for efficient image enhancement. In the framework established above the ADC performs two functions: (1) affine transformation $f_i(\cdot)$ and (2) digitization adc$(\cdot)$. First, a linear adc$(\cdot)$ corresponding to an ideal digitization process is considered. Next, an affine adc$(\cdot)$ for nonideal digitization seen in common ADCs is discussed.

2.1. *Ideal model*

The ADC converts the analog signal V to a digital image S. Region R_i of S (denoted by S_i) consists of gray values $s_{ij} \in \Phi$ obtained from analog signal value $v_{ij} \in \Theta$ by the ideal digitization process $s_{ij} = cv_{ij} + e$, where c is a scalar constant and e is a *nonlinear* quantization error. In most ADCs a common method of transforming input v_{ij} is by setting low and high analog offsets $(v_{ai}, v_{bi}) \in \Theta^2$. The algorithm processes S_i to automatically generate digital offsets $(s_{ai}, s_{bi}) \in \Phi^2$, which are transformed by the DAC to analog offsets $(v_{ai}, v_{bi}) \in \Theta^2$. Note that the DAC is included in almost all ADC hardware. The Offset Block $f_i(\cdot)$ (see Fig. 1) is described as below:

$$f_i(v_{ij}) = \begin{cases} v_{\max}, & v_{ij} \geq v_{bi} \\ \left(\dfrac{v_{\max} - v_{\min}}{v_{bi} - v_{ai}}\right)(v_{ij} - v_{ai}) + v_{\min}, & v_{ai} < v_{ij} < v_{bi}, \\ v_{\min}, & v_{ij} \leq v_{ai} \end{cases} \quad \text{for } i = 1, \ldots, m \text{ and } j = 1, \ldots, n_i. \tag{1}$$

The transformed input $f_i(v_{ij})$ is digitized to obtain the enhanced value $t_{ij} = \text{adc}(f_i(v_{ij})) \in T_i$. Here, t_{ij} are gray values within the enhanced image T_i. For an ideal digitization, ignoring quantization errors:

$$t_{ij} = g_i(s_{ij} - s_{ai}) + s_{\min}, \quad \text{for } i = 1, \ldots, m, \quad \text{and} \quad j = 1, \ldots, n_i, \text{ where } t_{ij} \in T_i. \tag{2}$$

Here, n_i is the number of pixels in S_i and g_i is the gain given by:

$$g_i = \frac{v_{\max} - v_{\min}}{v_{bi} - v_{ai}} = \frac{s_{\max} - s_{\min}}{s_{bi} - s_{ai}}, \quad \text{for } i = 1, \ldots, m. \tag{3}$$

Note that s_{ij} and t_{ij} represent the ideal digitized values of v_{ij} and $f_i(v_{ij})$, respectively. The actual gray values are a round-off (quantization) of the ideal

values. The effects of quantization and measurement errors in t_{ij} are shown in Section 4. From (2) we shall obtain equations for two different measures of S_i: (a) mean s_i, and (b) standard deviation $\sigma(s_i)$:

$$t_i = g_i(s_i - s_{ai}) + s_{\min}, \quad \text{for } i = 1, \ldots, m, \text{ and}$$
$$\sigma(t_i) = g_i\sigma(s_i), \quad \text{for } i = 1, \ldots, m. \tag{5}$$

Here t_i and $\sigma(t_i)$ are the mean and standard deviation, respectively, of T_i.

The above equations (4) and (5) have the following *constraints*:

(1) The linearity assumption of the digitization process in equation (2) is valid only for a range of $g_i \leq g_{\max}$, which is determined experimentally (see Appendix). We, therefore, obtain the range:

$$R(g_i): 1 \leq g_i \leq g_{\max}. \tag{6}$$

(2) Furthermore, we have $s_{bi} > s_{ai}$ and $(s_{ai}, s_{bi}) \in \Phi^2$. Constraint (2) can be expressed as:

$$R(s_{ai}): s_{\min} \leq s_{ai} \leq s_{\max} - \frac{s_{\max} - s_{\min}}{g_i}. \tag{7}$$

A plot of g_i versus s_{ai} in Fig. 2 for $s_{\min} = 0$ and $s_{\max} = 255$ shows a wider selection of low offset s_{ai} for higher values of gain g_i.

The final enhanced image $U_i = \{u_{ij}, j = 1, \ldots, n_i\}$ is generated by the weighted sum of images T_i with weights w_i and then clipped by the activation function act$(\cdot)$ to lie within $[s_{\min}, s_{\max}]$. Images $\{U_1, \ldots, U_m\}$ form regions $\{R_1, \ldots, R_m\}$, respectively, of final enhanced image U. Thus,

$$u_{ij} = \begin{cases} s_{\max}, & w_i t_{ij} \geq s_{\max}, \\ w_i t_{ij}, & s_{\min} < w_i t_{ij} < s_{\max}, \\ s_{\min}, & w_i t_{ij} \leq s_{\min} \end{cases} \quad i = 1, \ldots, m, j = 1, \ldots, n_i \text{ and } U = \bigcup_{i=1}^{m} U_i. \tag{8}$$

2.2. *Nonideal model*

In this section we shall modify the ideal model (2) to fit the nonidealities found many common ADCs. The nonidealities are considered both for the digitization process and the analog signal transformation in the Offset Block. Considering common nonidealities[30,32] and ignoring second-order error terms, we obtain the following expression for enhanced image T_i instead of equation (2):

$$t_{ij} = g_i s_{ij} + k_1 g_i s_{ai} + k_2 s_{ai} + k_3 s_{ij} + k_4,$$
$$\text{for } i = 1, \ldots, m, \text{ and } j = 1, \ldots, n_i, \text{ where } t_{ij} \in T_i. \tag{9}$$

Equations for mean and standard deviation are easily obtained from equation (9).

In equation (9) (k_1, k_2, k_3, k_4) are unknown real-valued model constants. The ideal values are: $k_1 = -1$, $k_2 = k_3 = 0$. Constant k_4 represents any bias in the system due to an affine ADC. Ideally for an unbiased system, $k_4 = s_{\min}$, which is usually 0.

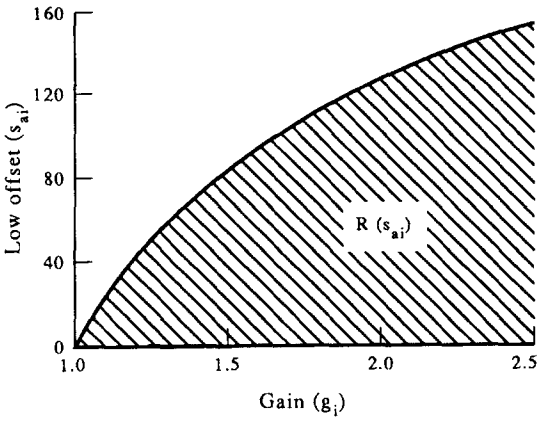

Fig. 2. Range of low offset s_{ai} for different gains g_i.

Perhaps it can be demonstrated that equation (9) can be derived by assuming nonidealities for other parameters or by assuming different nonidealities for the same parameters. However, our experiments (in Section 3.5) show that equation (9), independent of its derivation, appropriately represents the nonideal system under discussion.

3. ENHANCEMENT METHOD

The enhancement method consists of two steps: (1) an offline estimation of model constants (k_1, k_2, k_3, k_4) by the method in Section 3.1 and (2) an online estimation of the ADC offsets (s_{ai}, s_{bi}) and weights w_i, for $i = 1, \ldots, m$. The enhanced image is obtained by the algorithms in Sections 3.2 and 3.3.

3.1. *Offline estimation of model constants* (k_1, k_2, k_3, k_4)

Before estimating (k_1, k_2, k_3, k_4) we compute the upper limit $g_{\max}$ of gain g_i by the algorithm in the Appendix. We also identify m regions $\{R_1, \ldots, R_m\}$ for enhancement (see Appendix). From $g_{\max}$, we obtain the following inequality from equations (3) and (6):

$$s_{ai} + \frac{s_{\max} - s_{\min}}{g_{\max}} \leq s_{bi} \text{ and } (s_{ai}, s_{bi}) \in \Phi^2. \tag{10}$$

Estimate (k_1, k_2, k_3, k_4) as follows:

(1) For each region R_i, $i = 1, \ldots, m$, choose p offsets (s_{ak}, s_{bk}), $k = 1, \ldots, p$, within the constraint of equation (10) and compute gain g_k by equation (3). Here $p\,(>4)$ is an arbitrary number of offsets (say 10), such that the least-squares equation (11) below is overdetermined.

(2) For each (s_{ak}, s_{bk}), acquire an image and estimate t_{ik} by averaging gray values R_i. Note that t_{ik} can be obtained by other methods such as a weighted average, median or random sample of gray values within R_i. Eliminate those t_{ik} that are close to $s_{\min}$ and $s_{\max}$, thus satisfying equation (7).

(3) Equation (3) can be rewritten in the following matrix form for each region R_i:

$$[1 \quad s_{ak} \quad g_k s_{ak} \quad g_k] \begin{bmatrix} k_3 s_i + k_4 \\ k_2 \\ k_1 \\ s_i \end{bmatrix} = [t_{ik}],$$

$$i = 1, \ldots, m, k = 1, \ldots, p. \quad (11)$$

The above equation is solved by the least-squares method.

(4) Final estimates of (k_1, k_2) are obtained by averaging m estimates obtained from m regions.

(5) From m estimates of s_i and $(k_3 s_i + k_4)$, $i = 1, \ldots, m$, obtained from equation (11), compute k_3 and k_4 by the least-squares method.

3.2. *Online generation of enhanced image with desired mean gray value d_i*

Here we generate an enhanced image U from the user-specified mean gray value d_i for each region R_i, $i = 1, \ldots, m$. The analysis for user-specified desired standard deviation $\sigma(d_i)$ is considered in Section 3.3. Specifically, we estimate offsets (s_{ai}, s_{bi}) and weights w_i from: (1) known model constants (k_1, k_2, k_3, k_4) and (2) desired mean gray value d_i for each region R_i, $i = 1, \ldots, m$. The enhanced image T_i is obtained by modifying input V_i by estimated offsets (s_{ai}, s_{bi}). The final image U_i is obtained as $w_i T_i$. From equation (9), we have:

$$d_i = w_i(g_i s_i + k_1 g_i s_{ai} + k_2 s_{ai} + k_3 s_i + k_4),$$
$$i = 1, \ldots, m, \text{ where } d_i \in \Phi. \quad (12)$$

The solution to equation (12) is obtained under constraints (6) and (7). Clearly there is no unique solution for equation (12). We shall, therefore, obtain a solution that best suits the computational considerations and our model assumptions. Compute (g_i, s_{ai}) by the following iterative algorithm:

(1) Choose the starting value of $w_i = 1$.

(2) Choose the starting value of $g_i = 1$.

(3) Compute s_{ai} and check if s_{ai} satisfies the following condition [obtained from equations (12) and (7)]:

$$s_{ai} = \frac{d_i - w_i(g_i + k_3)s_i - w_i k_4}{w_i(k_1 g_i + k_2)} \in R(s_{ai}). \quad (13)$$

(4) If s_{ai} satisfies equation (13), report g_i, s_{ai} and w_i and terminate the algorithm.

(5) If s_{ai} does not satisfy equation (13), increment g_i (by say 0.1) and go back to step 3.

(6) Continue the iteration until $g_i = g_{\max}$. If $g_{\max}$ does not satisfy equation (13) check the following:

(6.1) If s_{ai} computed from equation (13) with $g_i = g_{\max}$ exceeds the upper limit in $R(s_{ai})$, then decrement w_i by 2^{-p}, where p is an integer (see Section 3.4).

(6.2) If s_{ai} computed from equation (13) with $g_i = g_{\max}$ is below the lower limit in $R(s_{ai})$, then increment w_i by 2^{-p}.

(7) Go back to step 2.

Note that the algorithm chooses the smallest value of $g_i \in R(g_i)$, because the linearity assumption of the ADC is strongest for g_i closest to 1. Furthermore, the algorithm chooses w_i closest to 1 since $w_i = 1$ is the most efficient solution. Parameter s_{bi} is obtained as:

$$s_{bi} = s_{ai} + \frac{s_{\max} - s_{\min}}{g_i}.$$

3.3. *Online generation of enhanced image with desired standard deviation $\sigma(d_i)$*

Here we shall modify the above algorithm to obtain both desired mean d_i and standard deviation $\sigma(d_i)$. From equation (12) we obtain:

$$\sigma(d_i) = w_i(g_i + k_3)\sigma(s_i). \quad (14)$$

The modified algorithm is:

(1) Choose the starting value of $w_i = 1$.

(2) Compute g_i from $g_i = (\sigma(d_i)/w_i\sigma(s_i)) - k_3$. Check if $g_i \in R(g_i)$.

(2.1) If $g_i \notin R(g_i)$ and $g_i < 1$, then reduce w_i by steps of 2^{-p} untill $g_i \in R(g_i)$.

(2.2) If $g_i \notin R(g_i)$ and $g_i > g_{\max}$, then increase w_i by steps of 2^{-p} untill $g_i \in R(g_i)$.

(3) Compute s_{ai} from equation (13) and check if $s_{ai} \in R(s_{ai})$ in equation (7).

(3.1) If $s_{ai} \in R(s_{ai})$, report (g_i, s_{ai}, w_i) and terminate the algorithm.

(3.2) If $s_{ai} \notin R(s_{ai})$ and $s_{ai} > \max_{s_{ai}} R(s_{ai})$, then reduce w_i by 2^{-p}.

(3.3) If $s_{ai} \notin R(s_{ai})$ and $s_{ai} < \min_{s_{ai}} R(s_{ai})$, then increase w_i by 2^{-p}.

(4) Go back to step 2.

Note that the algorithm may not have a solution, because w_i adjustments in steps 2 and 3 may be complementary. It is, therefore, necessary to explore the conditions under which solutions to the above algorithm exist.

Theorem 1. (for the ideal model). The necessary and sufficient condition for which solutions for g_i, s_{ai} and w_i exist for the ideal model for a given optical setup $(s_i, \sigma(s_i))$ and given desired values $(d_i, \sigma(d_i))$ is:

$$0 \le s_i - \left(\frac{\sigma(s_i)}{\sigma(d_i)}\right) d_i \le s_{\max} - \frac{s_{\max}}{g_{\max}}.$$

Proof. Recall that the expressions for d_i and $\sigma(d_i)$ are obtained for the ideal model by placing $(k_1 = -1, k_2 = k_3 = 0, k_4 = s_{\min})$ in equations (12) and

(14) as follows:

$$d_i = w_i g_i (s_i - s_{ai}) + w_i s_{\min}, \quad \text{and} \tag{12a}$$

$$\sigma(d_i) = w_i g_i \sigma(s_i). \tag{14a}$$

From equations (12a) and (14a) we obtain $s_{ai} = s_i - (d_i\sigma(s_i)/\sigma(d_i)) + (s_{\min}/g_i)$. Thus, the maximum value of s_{ai} is $s_i - (d_i\sigma(s_i)/\sigma(d_i)) + s_{\min}$ for $g_i = 1$. For s_{ai} to exist, this value should be greater than or equal to $s_{\min}$, which gives us $s_i - (d_i\sigma(s_i)/\sigma(d_i)) \geq 0$. Furthermore, the minimum value of s_{ai} is $s_i - (d_i\sigma(s_i)/\sigma(d_i)) + (s_{\min}/g_{\max})$ for $g_i = g_{\max}$. This value should be less than or equal to $s_{\max} - (s_{\max} - s_{\min})/g_{\max}$, which gives us $s_i - (d_i\sigma(s_i)/\sigma(d_i)) \leq s_{\max} - (s_{\max}/g_{\max})$. Conversely, if the above condition is satisfied, we obtain $s_{ai} \in R(s_{ai})$ and $g_i \in R(g_i)$, which gives us a valid solution. □

3.4. *Permissible range of desired mean d_i and standard deviation $\sigma(d_i)$ for $w_i = 1$*

Weights w_i are used in equations (12) and (14) to obtain any enhancement that cannot be obtained with $w_i = 1$. However, multiplication by $w_i \neq 1$ is inefficient and, therefore, we shall explore the enhancement that is possible with $w_i = 1$. We shall obtain a range $R(d_i)$ of d_i in order to obtain the desired enhancement with $w_i = 1$. Assuming that only desired mean is selected and $\sigma(d_i)$ is not selected by the user, we have from equation (12):

$$R(d_i): \min_{\substack{g_i \in R(g_i) \\ s_{ai} \in R(s_{ai})}} \{(g_i + k_3)s_i + (k_1 g_i + k_2)s_{ai} + k_4\} \leq$$

$$d_i \leq \max_{\substack{g_i \in R(g_i) \\ s_{ai} \in R(s_{ai})}} \{(g_i + k_3)s_i + (k_1 g_i + k_2)s_{ai} + k_4\}. \tag{15}$$

A plot of $R(d_i)$ for the ideal case ($k_1 = -1, k_2 = k_3 = 0$, $k_4 = s_{\min}$) is shown in Fig. 3 for $s_{\min} = 0, s_{\max} = 255$ and $g_{\max} = 2.5$. Here we observe that for $100 \leq s_i \leq 150$, we can obtain all values of d_i for $w_i = 1$, whereas for $s_i = 200$ we can only obtain $d_i \geq 125$. Note that the left and right slopes of $R(d_i)$ in Fig. 3 are $g_{\max}$. Thus, the choices of d_i are limited by the maximum possible gain $g_{\max}$ of the ADC.

For the range $R(\sigma(d_i))$ of $\sigma(d_i)$ with $w_i = 1$, we have:

$$R(\sigma(d_i)): \sigma(s_i)(1 + k_3) \leq \sigma(d_i) \leq \sigma(s_i)(g_{\max} + k_3). \tag{16}$$

It is clear from the above expression that the choices of $\sigma(d_i)$ are also limited by $g_{\max}$.

If both d_i and $\sigma(d_i)$ are specified by the user, then in order to determine $R(d_i)$ we replace g_i in equation (15) with $(\sigma(d_i)/\sigma(s_i)) - k_3$. Range $R(\sigma(d_i))$ in equation (16) is still valid. From the above expressions we observe that if our choices of d_i and $\sigma(d_i)$ cannot be attained with an ADC, then we can modify the optical setup to change s_i and $\sigma(s_i)$ such that d_i and $\sigma(d_i)$ satisfy equations (15) and (16), respectively.

Among the computations described above, it is the multiplication by w_i that makes it difficult to implement the method in digital hardware. In most image processors it is simpler to add or subtract images than to multiply an image. One possible way to solve this problem is to use powers-of-two weights, i.e. all weights can only take values on $\{0, 1, \pm 2^{-1}, \ldots, 2^{-p}\}$ such that the multipliers are replaced by shift registers. Here, p is an integer chosen according to the accuracy desired. A second method is to use a Look Up Table to map the digitized signal to a weighted gray value.

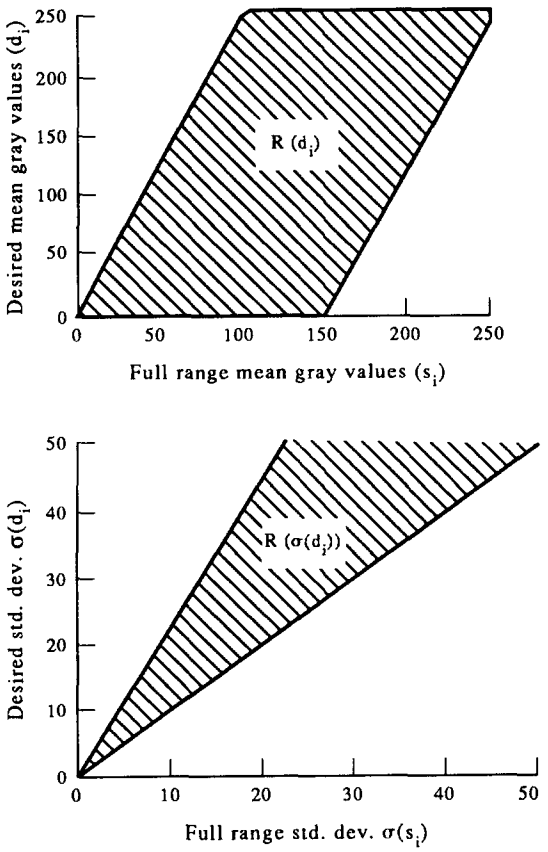

Fig. 3. Ranges $R(d_i)$ of desired mean d_i and $R(\sigma(d_i))$ of desired standard deviation $\sigma(d_i)$ for weight $w_i = 1$ and $g_{\max} = 2.5$.

3.5. *Experimental results*

In our experiments we have chosen an application of optical character recognition. The characters are laser etched on industrial samples of steel. Due to variations in the surface quality of the parts, we obtain a wide range of contrast (see Fig. 4). In order to segment the parts and characters we used the enhancement method to obtain a set of images with the *same* mean and standard deviation of gray values. The enhanced images are then segmented by the *same image processing algorithm*. This would not be possible with the original images.

The multiple parts and the background form regions $\{R_1, \ldots, R_m\}$ to be enhanced. First we estimated $g_{\max}$ from three different parts on a background. Figure 5 shows a plot of errors between the measured and computed gray values for different g_is for these parts.

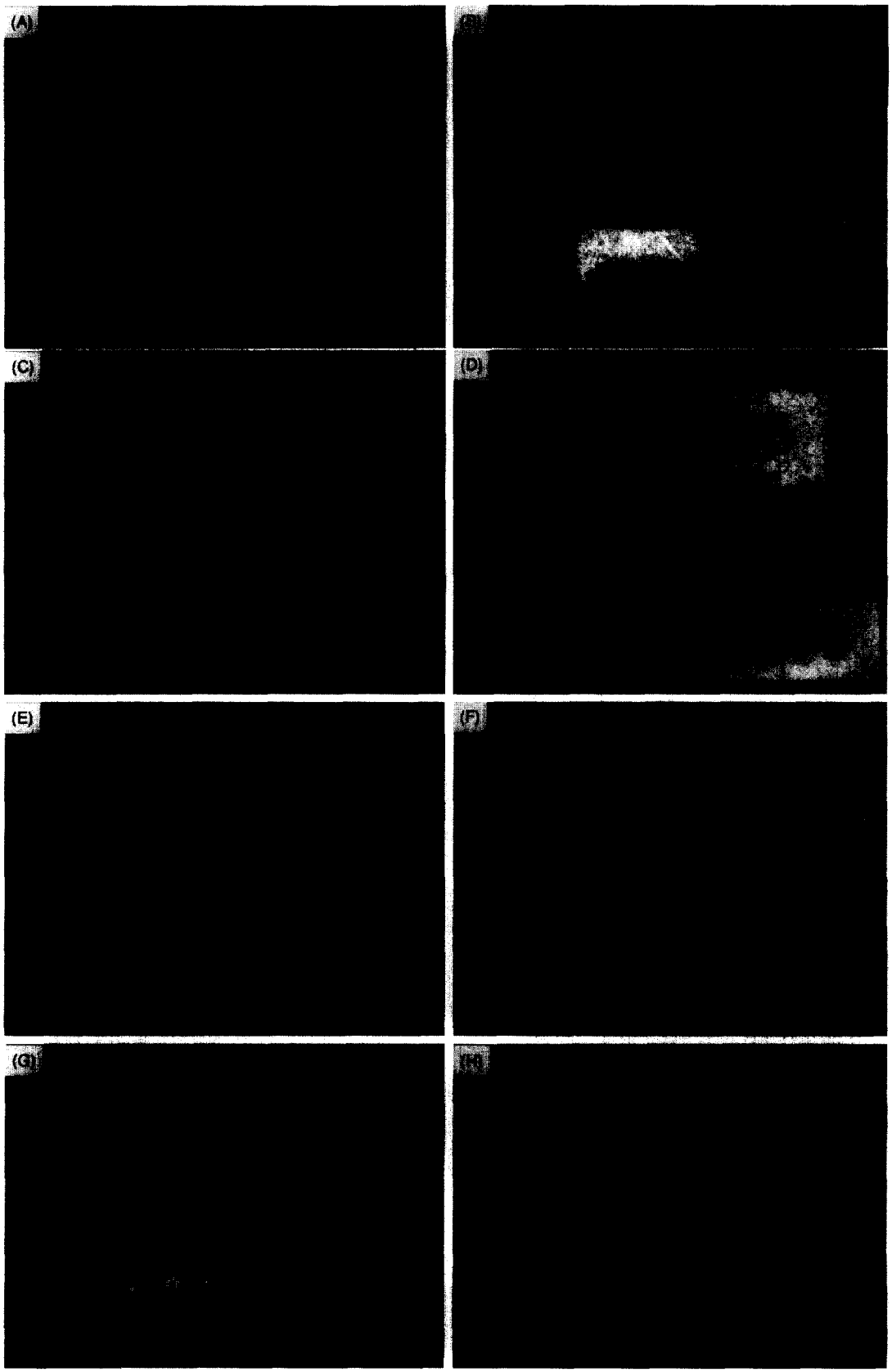

Fig. 4. (A), (C) and (E). Camera images of steel parts with varying contrast and laser-etched characters on them. (B), (D) and (F) Enhanced images with highlighted rectangular region in each part. The same segmentation algorithm is used in all parts to segment the characters. All characters in the enhanced regions are clearly segmented. (G) and (H). Gray-scale enhanced images for Figs. 4(A) and (E), respectively.

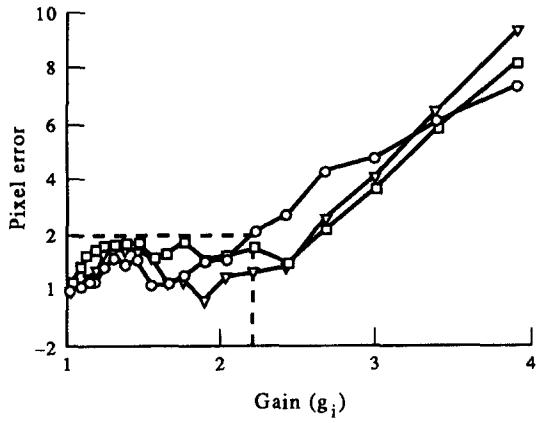

Fig. 5. Error in gray values for different gains.

Choosing a maximum error of two gray values, we estimated $g_{max} = 2.2$. The range of offsets (s_{ai}, s_{bi}) computed from equation (10) is: $(s_{ai} + 116) \leq s_{bi}$ and $(s_{ai}, s_{bi}) \in \Phi^2$.

First the model constants (k_1, k_2, k_3, k_4) are estimated by the offline algorithm in Section 3.1. From this experiment, we observe the following (see Tables 1 and 2):

(1) Estimates of (k_1, k_2, k_3) are close to their ideal values of $k_1 = -1$, $k = k_3 = 0$.

(2) Estimates of bias constant k_4 are different from their ideal value of $s_{min} = 0$. This deviation shows that the nonideal model (9) is a more accurate representation of the ADC than the ideal model (2). Thus, nonideal model gives us accurate enhanced images that cannot be obtained with the ideal model.

We applied the enhancement method on six different steel parts. Figures 4(A), (C) and (E) show the six parts with very different surface textures and also different contrast of the etched characters. Rectangular regions around some of these characters are identified for enhancement. For example, in Fig. 4(B) the rectangular regions enclose the characters "111" and "208" in the top and bottom parts, respectively. In Fig. 4(D) the rectangular regions enclose the characters "523" and "9011", which are enhanced. In Fig. 4(F) the rectangular regions enclose the characters "10" and "11", which are enhanced. The remaining characters in all images are not enhanced.

By using the enhancement method on each region separately, we obtained an enhanced image of the characters in Figs. 4(B), (D) and (F), respectively. All images are enhanced to the same desired mean $d_i = 150$ and desired standard deviation $\sigma(d_i) = 30$. A segmentation algorithm is then applied to the gray-scale enhanced images. We used the *same segmentation algorithm* for all images. The segmentation algorithm consists of gray-scale closing, thresholding, reduction, filtering and a binary closing in this sequence. The results show that the characters in the enhanced regions are always clearly segmented.

In another experiment, we computed the error between desired mean gray value d_i and enhanced mean gray value u_i for d_i between 50 and 200. We also computed the error between desired standard deviation $\sigma(d_i)$ and enhanced standard deviation $\sigma(u_i)$ for

Table 1. Estimates of model constants (k_1, k_2, k_3, k_4), gain g_1, offset $(\hat{k}_1\hat{g}_1 + \hat{k}_2)\hat{s}_{a1}$ and enhanced mean gray values $(\hat{u}_1, \hat{u}_2)$ due to a constant additive noise e in image S

e	$\hat{k}_1$	$\hat{k}_2$	$\hat{k}_3$	$\hat{k}_4$	$\hat{s}_1$	$\hat{s}_2$	$\hat{g}_1$	$(\hat{k}_1\hat{g}_1 + \hat{k}_2)\hat{s}_{a1}$	$\hat{u}_1$	$\hat{u}_2$
0	−1.0284	−0.0106	0.0550	−6.0056	114.15	36.42	1.2462	−2.3458	140.54	38.75
1	−1.0044	−0.0374	0.0550	−5.1488	113.95	36.64	1.2448	−3.4468	140.59	38.57
2	−1.0210	−0.0210	0.0542	−3.9058	114.03	36.55	1.2496	−4.5358	140.33	38.65
3	−1.0110	−0.0378	0.0582	−3.0118	113.92	36.59	1.2512	−5.5780	140.62	38.61
4	−1.0300	−0.0180	0.0496	−1.6976	114.18	36.74	1.2566	−7.0020	140.70	38.77
5	−1.0354	−0.0056	0.0564	−1.1598	113.84	36.84	1.2586	−8.1618	140.84	38.45
10	−1.0196	−0.0244	0.0518	4.2660	114.31	36.69	1.2474	−12.5842	140.72	38.47
Mean	−1.0214	−0.0211	0.0543		114.05	36.64	1.2506		140.62	38.61
SD	0.0110	0.0130	0.0029		0.1678	0.136	0.0052		0.1610	0.125

Table 2. Estimates of model constants (k_1, k_2, k_3, k_4), offset $(\hat{k}_1\hat{g}_1 + \hat{k}_2)\hat{s}_{a1}$, and enhanced mean gray values $(\hat{u}_1, \hat{u}_2)$ due to i.i.d. $N(0, \rho)$ additive noise in image S

ρ	$\hat{k}_3\hat{s}_1 + \hat{k}_4$	$\hat{k}_3\hat{s}_2 + \hat{k}_4$	$\hat{k}_2$	$\hat{k}_1$	$\hat{s}_1$	$\hat{s}_2$	$(\hat{k}_1\hat{g}_1 + \hat{k}_2)\hat{s}_{a1}$	$\hat{u}_1$	$\hat{u}_2$
0.00	0.4617	−4.1990	0.0179	−1.0272	102.94	36.39	−9.7959	140.90	38.56
0.25	0.4593	−4.3741	0.0157	−1.0531	103.40	36.45	−9.6275	140.89	38.63
0.50	0.3666	−4.0243	0.0177	−1.0151	103.32	36.22	−9.4418	140.96	38.68
0.75	0.4338	−4.2577	0.0087	−1.0406	103.49	36.33	−9.2059	140.49	38.57
1.00	0.4824	−4.2032	0.0122	−1.0260	103.76	36.43	−9.4128	140.91	38.42
1.25	0.4661	−4.1419	0.0075	−1.0463	102.88	36.11	−9.4729	140.92	38.51
1.50	0.3524	−4.2032	0.0073	−1.0366	103.45	36.40	−9.5164	140.76	38.44
Mean	0.4318	−4.2005	0.0124	−1.0350	103.32	36.33	−9.4962	140.83	38.54
SD	0.0516	0.1064	0.0047	0.0131	0.3115	0.123	0.1836	0.1636	0.094

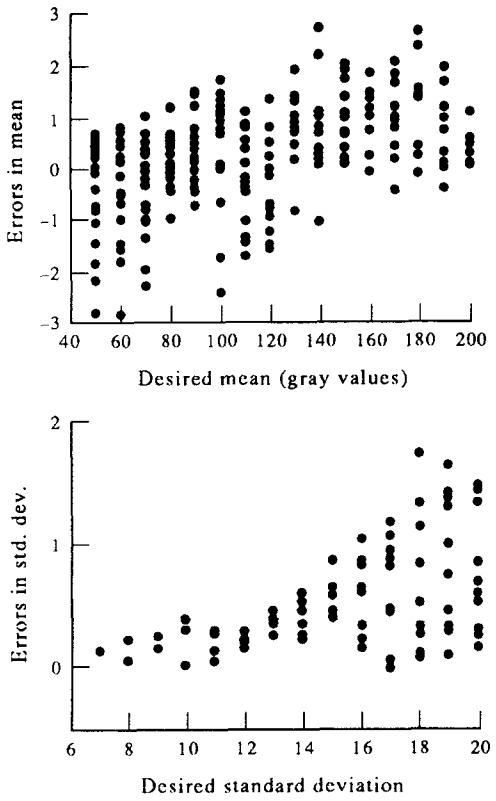

Fig. 6. Errors in mean u_i and standard deviation $\sigma(u_i)$ for enhanced image U.

$\sigma(d_i)$ between 7 and 40. Figure 6 shows that we have small errors (within ± 3) in u_i and $\sigma(u_i)$ with our models.

3.6. *Use of a single gain, offset and weight for simultaneous enhancement of two regions*

An obvious simplification of the proposed idea is the use of a single gain and offset for the entire image. This is the most common application of ADC's gain and offset, where the user sets them *manually* to obtain an enhanced image. Furthermore, a single weight w is used for the entire image. Although the method is fast and accurate, Theorem 2 below explores the limit of the number of regions that can be simultaneously enhanced by this method. Equation (12) is simplified to the following:

$$d_i = w(gs_i + k_1 g s_a + k_2 s_a + k_3 s_i + k_4) \quad \text{for } i = 1, \ldots, m. \tag{17a}$$

Theorem 2. The necessary and sufficient condition for which solutions for g, s_a and w exist in equation (17a) is:

$$\frac{d_i - d_j}{s_i - s_j} = \frac{d_k - d_r}{s_k - s_r}, \quad \text{for all } i, j, k, r = 1, \ldots, m \text{ such that } i \neq j \text{ and } k \neq r. \tag{17b}$$

Proof. For any pair of equations indexed by i and j, the solutions to equation (17a) are:

$$\alpha_{ij} = w(g + k_3) = \frac{d_i - d_j}{s_i - s_j},$$

$$\beta_{ij} = w((k_1 g + k_2)s_a + k_4) = d_i - s_i\left(\frac{d_i - d_j}{s_i - s_j}\right). \tag{17c}$$

If equation (17a) has a solution then $\alpha_{ij} = \alpha_{kr}$ and $\beta_{ij} = \beta_{kr}$. Considering only α_{ij} and α_{kr} we obtain equation (17b). Next we shall show that if equation (17b) is true, then equation (17a) has a solution. In other words, we have to show that $\beta_{ij} = \beta_{kr}$ and $\alpha_{ij} = \alpha_{kr}$ if equation (17a) is true. Clearly, from equations (17a) and (17c) $\alpha_{ij} = \alpha_{kr}$. From equation (17c) $\beta_{ij} - \beta_{kr} = (d_i - d_k) - c(s_i - s_k)$, where:

$$c = \frac{d_i - d_j}{s_i - s_j} = \frac{d_k - d_r}{s_k - s_r} = \frac{d_i - d_k}{s_i - s_k}.$$

From this equation we conclude : $\beta_{ij} - \beta_{kr} = 0$. Therefore, $\beta_{ij} = \beta_{kr}$. □

Theorem 2 shows that we can choose only two independent values of d_i for an image, the rest of which are fixed by equation (17b). This result is intuitive, since we have only two parameters (s_a, s_b) to modify input V. We can, therefore, independently choose only two regions for simultaneous enhancement, i.e. $m = 2$.

Further limitations of this simplified method are: (1) the range of the desired mean gray value obtained with this method is quite small, even after choosing any weight w, whereas the proposed method can be used to obtain any desired mean gray value in the enhanced image; (2) we cannot obtain a desired standard deviation in the enhanced image with this simple method. Desired mean gray values from the two regions are used to compute g and s_a.

4. ERROR ANALYSIS

In this section we shall determine: (1) errors in the estimation of model constants (k_1, k_2, k_3, k_4) due to nonlinear quantization and measurement errors in digitized gray values and (2) errors in the enhanced gray scale image U due to errors in model constants (k_1, k_2, k_3, k_4).

4.1. *Effects of quantization and measurement errors on model constants*

Let us assume an additive quantization and measurement error e_{ik} in the estimate $\hat{t}_{ik}$ of t_{ik} in equation (11):

$$\hat{t}_{ik} = t_{ik} + e_{ik}, \quad \text{for } i = 1, \ldots, m \text{ and } k = 1, \ldots, p.$$

Let $(\hat{k}_1, \hat{k}_2, \hat{k}_3, \hat{k}_4)$ and $\hat{s}_i$ be the estimates of (k_1, k_2, k_3, k_4) and s_i, respectively. From equation (11) we obtain:

$$\hat{k}_3\hat{s}_i + \hat{k}_4 = k_3 s_i + k_4 + a_{11}\sum_{k=1}^{p} e_{ik} + a_{12}\sum_{k=1}^{p} s_{ak} e_{ik}$$

$$+ a_{13} \sum_{k=1}^{p} g_k s_{ak} e_{ik} + a_{14} \sum_{k=1}^{p} g_k e_{ik},$$

$$\hat{k}_2 = k_2 + a_{21} \sum_{k=1}^{p} e_{ik} + a_{22} \sum_{k=1}^{p} s_{ak} e_{ik}$$

$$+ a_{23} \sum_{k=1}^{p} g_k s_{ak} e_{ik} + a_{24} \sum_{k=1}^{p} g_k e_{ik},$$

$$\hat{k}_1 = k_1 + a_{31} \sum_{k=1}^{p} e_{ik} + a_{32} \sum_{k=1}^{p} s_{ak} e_{ik}$$

$$+ a_{33} \sum_{k=1}^{p} g_k s_{ak} e_{ik} + a_{34} \sum_{k=1}^{p} g_k e_{ik},$$

$$\hat{s}_i = s_i + a_{41} \sum_{k=1}^{p} e_{ik} + a_{42} \sum_{k=1}^{p} s_{ak} e_{ik}$$

$$+ a_{43} \sum_{k=1}^{p} g_k s_{ak} e_{ik} + a_{44} \sum_{k=1}^{p} g_k e_{ik},$$

$$i = 1, \ldots, m. \quad (18)$$

In equation (18) $[a_{ij}]$, $i, j = 1, \ldots, 4$, are terms of the pseudoinverse matrix in the least-squares solution of equation (11). Further analyses for these equations are carried out under the assumption of: (a) a constant quantization error and (b) a Gaussian-independent identical distribution of quantization errors e_{ik}.

By assuming an additive constant quantization error e for t_{ik}, where e is the average of all errors e_{ik}, $i = 1, \ldots, m$, $k = 1, \ldots, p$, we obtain the following:

$$\hat{k}_1 = k_1, \hat{k}_2 = k_2, \hat{k}_3 = k_3, \hat{k}_4 = k_4 + e,$$
$$\hat{s}_i = s_i \text{ for } i = 1, \ldots, m. \quad (19)$$

It is clear from equation (19) that an additive constant quantization error has most effect on the estimate of the bias constant k_4 and no effect on the estimates of model constants k_1, k_2, k_3 and gray value s_i.

Assuming the quantization errors e_{ik} are i.i.d. $N(0, \rho)$ we obtain the following distributions:

$$\hat{k}_1 \sim N(k_1, \rho a_{33}), \hat{k}_2 \sim N(k_2, \rho a_{22}),$$
$$\hat{k}_3 \hat{s}_i + \hat{k}_4 \sim N(k_3 s_i + k_4, \rho a_{11}), \hat{s}_i \sim N(s_i, \rho a_{44}),$$
$$i = 1, \ldots, m. \quad (20)$$

These results show that the estimates are unbiased, have Gaussian distributions and their variances are proportional to error variance ρ.

4.2. *Error analysis for enhanced image U*

Here we shall determine errors in the enhanced image U, due to errors in model constants (k_1, k_2, k_3, k_4). The analyses are carried out under the assumptions of: (a) a constant quantization error e and (b) a Gaussian i.i.d. distribution of quantization errors e_{ik}.

Let $\hat{s}_{ai}$ be the estimate of s_{ai} in equation (13). For a constant quantization error e, we obtain from equation (13):

$$(\hat{k}_1 \hat{g}_i + \hat{k}_2)\hat{s}_{ai} = (k_1 g_i + k_2) s_{ai} - e. \quad (21)$$

Furthermore, the estimated sample standard deviation $\hat{\sigma}(s_i) = \sigma(s_i)$. Thus, from equation (14) we obtain:

$$\hat{g}_i = \frac{\sigma(d_i)}{w_i \hat{\sigma}(s_i)} - \hat{k}_3 = \frac{\sigma(d_i)}{w_i \sigma(s_i)} - k_3 = g_i. \quad (22)$$

From $(\hat{s}_{ai}, \hat{g}_i)$ above and equations (8) and (9), we obtain:

$$\hat{\sigma}(u_i) = w_i(\hat{g}_i + \hat{k}_3)\hat{\sigma}(s_i) = \sigma(d_i) \text{ and}$$
$$\hat{u}_i = d_i, \text{ for } i = 1, \ldots, m. \quad (23)$$

Thus, a constant quantization error e will cause no error in the final enhanced image U.

Next we assume i.i.d. $N(0, \rho)$ errors e_{ik}. From equations (13) and (20) we obtain the following distribution:

$$(\hat{k}_1 \hat{g}_i + \hat{k}_2)\hat{s}_{ai} = (k_1 g_i + k_2) s_{ai} - e_1 - e_2, \text{ where}$$
$$e_1 \sim N(0, g_i^2, \rho a_{44}) \text{ and } e_2 \sim N(0, \rho a_{11}). \quad (24)$$

Here, (e_1, e_2) are mutually correlated errors with unknown correlation coefficient. Substituting equations (24) and (20) into (8) and (9) we obtain: $\hat{u}_i = d_i$, for $i = 1, \ldots, m$. The estimated sample variance $\hat{\sigma}(s_i)^2$ is:

$$\hat{\sigma}(s_i)^2 = \sigma(s_i)^2 + \left(\frac{\rho}{n_i - 1}\right) e_1 + e_2,$$

where

$$e_1 \sim \chi^2_{n_i - 1} \quad \text{and} \quad e_2 \sim N(0, .). \quad (25)$$

Here, n_i is the number of pixels in R_i. From equations (13), (14), (8) and (9) we obtain: $\hat{\sigma}(u_i) = \sigma(d_i)$. Thus, i.i.d. $N(0, \rho)$ quantization error will cause no error in the final enhanced image U.

4.3. *Experiments on error analysis*

In these experiments, we have considered a single part on a background and enhanced the part with respect to the background. Two types of noise are added to the image: (a) constant additive noise e and (b) i.i.d. $N(0, \rho)$ additive noise. Tables 1 and 2 summarize the results.

Table 1 shows that $(\hat{k}_1, \hat{k}_2, \hat{k}_3)$ and $(\hat{s}_1, \hat{s}_2)$ have low standard deviations, suggesting small changes due to different amounts of contant noise e, whereas bias constant k_4 has an additive error e [see equation (19)]. Furthermore, estimates of g_1 have low standard deviation suggesting small variation [see equation (22)] due to constant noise e, whereas $(\hat{k}_1 \hat{g}_1 + \hat{k}_2)\hat{s}_{a1}$ has an additive error $-e$ as shown in equation (21). The final enhanced image U has small errors as indicated by low standard deviations.

Next, we add i.i.d. $N(0, \rho)$ noise in S. We repeated the experiment 50 times for each noise variance ρ and averaged the results to generate the final results in Table 2.

Table 2 shows that estimates of (k_1, k_2, k_3, k_4) and (s_1, s_2) have low standard deviations for different amounts of i.i.d. Gaussian noise supporting equation (20), i.e. the mean is unbiased. Finally, the enhanced

image $(\hat{u}_1, \hat{u}_2)$ has low standard deviations, suggesting small errors due to i.i.d. Gaussian noise in S.

5. CONCLUDING REMARKS

In this study we have discussed a new method of hybrid image enhancement, which can be easily implemented using the ADC that is commonly found in most image processors. The method is efficient and since its implementation does not require any additional hardware, it is inexpensive. The method has been used to enhance images of characters that are laser etched on steel with varying surface properties. Different samples of steel are enhanced to the same mean and standard deviation of gray values such that they can be segmented by a single algorithm. A simplified version of the algorithm is also suggested in Section 3.6. Details of this simplification along with its limitations are discussed in a separate study.[30,32]

REFERENCES

1. ADS-927, 1MHz, 14-bit, Low Power Sampling A/D Converter, Datel Inc. International, Tokyo, Japan.
2. Bt253, 18MSPS Monolithic CMOS Triple-Chan. 8-bit Image Digitizer, Brooktree Corporation, San Diego, California.
3. MP7684A, Monolithic CMOS 8-bit A-to-D Flash Converter, Micro Power Systems Inc., Santa Clara, California.
4. W. B. Green, *Digital Image Processing: A System Approach*. Van Nostrand Reinhold, New York (1983).
5. R. C. Gonzalez and P. Wintz, *Digital Image Processing*. Addison-Wesley, Massachussetts (1987).
6. T. S. Huang, Image enhancement: a review, *Opto-Electronics* **1**, 49–59 (1969).
7. A. K. Jain, *Fundamentals of Digital Image Processing*. Prentice Hall, New Jersey (1989).
8. J. S. Lim, *Two-Dimensional Signal and Image Processing*. Prentice-Hall, New Jersey (1990).
9. W. K. Pratt, *Digital Image Processing*, 2nd edn. Wiley, New York (1991).
10. J. C. Russ, *The Image Processing Handbook*. CRC Press, Boca Raton, Florida (1992).
11. E. Alparslan and F. Ince, Image enhancement by local histogram stretching, *IEEE Trans. Syst., Man Cybernet.* **11**(5), 376–385 (May 1981).
12. A. Beghdadi and Le Negrate, Contrast enhancement technique based on local detection of edges, *Comput. Vis. Graphics Image Process.* **46**, 162–174 (1989).
13. R. Cromartie and S. M. Pizer, Structure-sensitive adaptive contrast enhancement methods and their evaluation, *Image Vis. Comput.* **11**(8), 460–467 (1993).
14. R. Dale-Jones and T. Tjahjadi, Four algorithms for enhancing images with large peaks in their histogram, *Image Vis. Comput.* **10**(7), 495–507 (1992).
15. W. Frei, Image enhancement by histogram hyperbolization, *Comput. Graphics Image Process.* **6**, 286–294 (1977).
16. R. C. Gonzalez and B. A. Fittes, Gray level transformations of interactive image enhancement, *Mechanism Mach. Theory* **12**, 111–122 (1977).
17. R. Gordon, Enhancement of mammographic features by optimal neighborhood image processing, *IEEE Trans. Med. Imaging* **5**(1), 8–15 (1986).
18. J. L. Harris Jr, Constant variance enhancement: a digital processing technique, *Appl. Optics* **16**, 1268–1271 (1977).
19. T. S. Huang, *Two-Dimensional Digital Signal Processing I and II, Topics in Applied Physics*, Vols. 42–43. Springer Verlag, Berlin (1981).
20. R. A. Hummel, Image enhancement by histogram transformation, *Comput. Vis. Graphics Image Process.* **6**, 184–195 (1977).
21. R. A. Hummel, Histogram modification techniques, *Comput. Vis. Graphics Image Process.* **4**, 209–224 (1975).
22. J. Kautsky, D. L. B. Jupp and N. K. Nichols, Smoothed histogram modification for image processing, *Comput. Vis., Graphics Image Process.* **26**, 271–291 (1984).
23. K. Rehm, G. W. Seely, W. J. Dallas, T. W. Ovitt and J. F. Seeger, Design and testing of artifact-suppressed adaptive histogram equalization: A contrast-enhancement technique for the display of digital chest radiographs. *J. Theoracic Imaging* **5**(1), 85–91 (1990).
24. S. M. Pizer E. P. Amburn, J. D. Austin, A. Geselowitz, T. Greer, B. H. Ronenrj, J. B. Zimmerman and K. Zvitterveld, Adaptive histogram equalization and its variations, *Comput. Vis., Graphics Image Process.* **39**, 355–368 (1987).
25. V. Kim and L. Yaroslavskii, Rank algorithms for picture processing, *Comput. Vis., Graphics Image Process.* **35**, 234–258 (1986).
26. W. Morrow, W. Paranjape, R. B. Rangayyan and R. M. Desautels, Region-based contrast enhancement of mammograms, *IEEE Trans. Med. Imaging* **11**(3), 393–406 (1986).
27. K. W. Leszczynski and S. Shalev, A robust algorithm for contrast enhancement by local histogram modification, *Image Vis. Comput.* **7**(3), 205–209 (1989).
28. IEEE Proceedings, Computer and Digital Techniques (Special Issue on Image Restoration and Enhancement), Vol. **127**, pp. 5 (September 1980).
29. J. S. Lee, Digital image enhancement and noise filtering by use of local statistics, *IEEE Trans. Pattern Anal. Mach. Intell.* **2**(2), 165–168 (March 1980).
30. C. Chatterjee and V. P. Roychowdhury, Efficient image processing algorithms for enhanced desired gray scale images, *Proc. SPIE's Int. Symp. Optics, Imaging Instrument*. San Diego, California (11–16 July 1993).
31. K. S. Fu and J. K. Mui, A survey on image segmentation, *Pattern Recognition* **13**, 3–16 (1981).
32. C. Chatterjee and V. P. Roychowdhury, A real-time hybrid image enhancement method, Purdue University Technical Report (1995).

APPENDIX

Estimation of maximum gain $g_{\max}$

In order to maintain the linearity assumptions in equations (2) and (9), we determine the operating ranges for offsets s_{ai} and s_{bi}. For this, we determine the upper limit $g_{\max}$ for gain g_i as follows:

(1) Select $m (\geq 2)$ regions of interest $\{R_1, \ldots, R_m\}$ within the image (see below).

(2) Start from the first region R_1, i.e. $i = 1$, where index i is the ith estimate of $g_{\max}$ from region R_i.

(3) Choose a large starting value g_{start} (say 4) of $g_{\max}$ such that the estimate of $g_{\max}$ is expected to be less than g_{start}. Now estimate constants (k_1, k_2, k_3, k_4), see Section 3.1.

(4) Choose a set of p (>4) offsets (s_{ak}, s_{bk}), $k = 1, \ldots, p$, satisfying equation (7).

(5) For each choice of offset (s_{ak}, s_{bk}), $k = 1, \ldots, p$, perform the following steps:

(5.1) Acquire an image with offsets (s_{ak}, s_{bk}).

(5.2) From this acquired image measure gray value t_{ik_meas} by averaging gray values within R_i. Eliminate values that are close to $s_{\min}$ and $s_{\max}$.

(5.3) Compute gray value t_{ik_comp} from equation (9).

(5.4) Compute the pixel error (e_{ik}) as: $e_{ik} = t_{ik\_\text{meas}} - t_{ik\_\text{comp}}$.

(5.5) Compute gain g_{ik} from equation (3).

(6) Choose a limit e_{max} (say 2 pixels) of e_{ik}, $k = 1, \ldots, p$, and estimate the upper limit $g_{max}^{R_i}$ of g_i.

(7) If $g_{max}^{R_i} < g_{start}$, then set $g_{start} = g_{max}^{R_i}$ and repeat steps 4–7 untill $g_{max}^{R_i} = g_{start}$.

(8) If $g_{max}^{R_i} = g_{start}$, then report $g_{max}^{R_i}$ as the estimate of g_{max} from region R_i.

(9) Repeat steps 3–8 for all selected regions $\{R_1, \ldots, R_m\}$.

(10) Choose the final estimate g_{max} as the minimum value of all estimates: $g_{max} = \min_{i=1,\ldots,m} \{g_{max}^{R_i}\}$.

Selection of region $\{R_1, \ldots, R_m\}$

The m regions $\{R_1, \ldots, R_m\}$ are usually chosen by predefined criteria based upon the application. For example, in an image with multiple parts on a background, each part and the background forms regions $\{R_1, \ldots, R_m\}$. Instead of using the entire region R_i for parameter estimation, a small probing window within R_i is chosen to reduced computation.

About the Author—CHANCHAL CHATTERJEE received the B.Tech. degree in Electrical engineering from the Indian Institute of Technology, Kanpur, India and the M.S.E.E. degree from Purdue University, West Lafayette, IN, in 1983 and 1984, respectively. Between 1985 and 1995 he worked at Machine Vision International and Medar Inc. both at Detroit, MI. In 1996, he received the Ph.D. degree in Electrical engineering from Purdue University, West Lafayette, IN. He is currently a Research Associate in the School of Electrical and Computer Engineering at Purdue University. His areas of interest include image processing, computer vision and neural networks, and adaptive algorithms and systems per pattern recognition and digital communications.

About the Author—VWANI P. ROYCHOWDHURY received the B.Tech. degree from the Indian Institute of Technology, Kanpur, India, and the Ph.D. degree from Stanford University, Stanford CA, in 1982 and 1989, respectively, all in electrical engineering. He is currently an associate professor in the School of Electrical and Computer Engineering at Purdue University. From September 1989 to August 1991 he held a research associateship position in the Department of Electrical Engineering at Stanford University. His research interests include parallel algorithms and architectures, computational paradigms for nanoelectronics, design and analysis of neural networks, special purpose computing arrays, VLSI design and fault-tolerant computation.